Two regimes of the equatorial warm pool.

Part I: A simple tropical climate model

Masahiro Watanabe[1]

Faculty of Environmental Earth Science, Hokkaido University

Journal of Climate

Submitted on July 19, 2007

Revised on December 6, 2007

Corresponding author:

M. Watanabe, Faculty of Environmental Earth Science, Hokkaido University

N10W5, Sapporo, Hokkaido 060-0810, Japan

E-mail: hiro@ees.hokudai.ac.jp

---

[1] Present affiliation: Center for Climate System Research, University of Tokyo. 5-1-5 Kashiwanoha, Kashiwa, Chiba, Japan

ABSTRACT

Atmosphere-ocean coupled processes responsible for generating and maintaining the equatorial warm pool were investigated by means of models of different complexity. A primary focus is to clarify the question why the observed warm pool is concentrated around the maritime continent. In this Part I, solutions of a simple conceptual model which represents the tropical Pacific and Indian Oceans interacting via the Walker circulation are examined. When the inter-basin coupling is sufficiently strong, surface wind convergence over the maritime continent associated with easterly trades over the Pacific acts to generate the equatorial westerly over the Indian Ocean, leading to a warm pool spontaneously emerging between the two ocean basins. The conceptual model shows that tropical climate has two equilibria depending upon the ocean basin widths: a single warm pool regime corresponding to current climate and a split warm pool regime which accompanies warm pools created at the western parts of each ocean basin. The latter is found to be unstable and hence exhibit large-amplitude vacillations between the ocean basins, being further amplified by the Bjerknes feedback. The above two regimes of the equatorial warm pool are identified in the model incorporating the interactive Atlantic Ocean as well, in which the mean state and variability in the three ocean basins qualitatively agree with observations.

1. Introduction

Despite the fact that the insolation at the top of the atmosphere is independent of longitude, tropical climate as represented by sea surface temperature (SST) has considerable zonal non-uniformity. In particular, the existence of the warm pools which drive the general circulation of the atmosphere is peculiar; they are characterized by regions of relatively uniform SST higher than 28 °C spreading around the maritime continent and the western tropical Atlantic (Fig. 1, top). Two fundamental properties of the warm pools that have been discussed in the literature are the spatial homogeneity and the longitudinal placement, the latter contrasting with the presence of cold tongues in the eastern basin (e.g., Clement et al. 2005).

The spatial homogeneity of the warm pool, as frequently represented by the negatively skewed probability distribution of tropical SST, suggests that processes which prohibit rising of SST are at work. The primary candidate is the cirrus cloud which reflects the solar radiation and hence acts as thermostat for the ocean surface (Ramanathan and Collins 1991; Ramanathan et al. 1995). Subsequently, the importance of other processes was suggested: negative feedbacks due, for example, to the surface evaporation (Hartmann and Michelsen 1993) and the tropospheric relative humidity (Pierrehumbert 1995). All of these are atmospheric processes, so that a bulk argument of the atmospheric net heat transport regulating the warm pool SST is also possible (Wallace 1992), which may in turn be constrained by the oceanic heat transport mostly due to the Ekman drift (Held 2001).

Apart from its homogeneity, the warm pool is regarded as the surface manifestation of warm water piled up in the equatorial upper ocean (Fig. 1, middle). This necessarily accompanies a zonal tilt in thermocline, deeper (shallower) in the west

(east) both in the Pacific and the Atlantic, which is also associated with the existence of cold tongues in the eastern basin. Over the past decades, it has been elucidated that this climatological state is responsible for the El Niño-Southern Oscillation (ENSO). In short, a perturbed wind stress gives rise to changes in ocean upwelling and thermocline tilt both of which favorably affect the cold tongue SST. The resultant change in zonal SST gradient works to intensify the initial wind stress anomaly via modulating the atmospheric zonal differential heating. This is the heart of the Bjerknes (1969) feedback on which the ENSO amplification relies. The thermocline change is dominated by the slow ocean dynamical adjustment, which provides a timescale of ENSO (Neelin et al. 1998 and references therein).

Not only ENSO but the climatological east-west contrast in SST and thermocline depth can now be understood with the same mechanism, sometimes called the "climatological version" of the Bjerknes feedback (Neelin and Dijkstra 1995; Jin 1996). Dijkstra and Neelin (1995), using an intermediate coupled model for the tropical Pacific, have shown that the warm pool-cold tongue pattern considerably varies in the model with different sets of parameters, such as the efficiency of the upwelling and the thermocline on SST and the magnitude of the wind stress response to the zonal SST gradient, all controlling the climatological Bjerknes feedback. Jin (1996, referred to as J96 hereinafter) has demonstrated that a coupled system similar to but simpler than that of Dijkstra and Neelin (1995), which is also used in this study, can explain both the climatological state and ENSO in terms of the bifurcation of the equilibrium solution from stable to unstable branches.

The role of the ocean dynamical adjustment has been discussed even in terms of regulating the warm pool SST to an upper bound (Sun and Liu 1996; Clement et al.

1996; Seager and Murtugudde 1997). Li et al. (2000) and Clement et al. (2005) quantified the relative role of the feedbacks due to cloud, evaporation and ocean dynamics using an intermediate coupled model. Except for some differences in the detail, both studies conclude that all those processes are of importance for regulating the warm pool SST.

Observations reveal that the Pacific warm pool is smoothly extended into the eastern Indian Ocean (cf. Fig. 1), which has been less focused in the above studies with few exceptions (e.g., Schneider et al. 1996). The diabatic heating over the maritime continent driving the easterly winds over the Pacific would necessarily force the equatorial westerlies over the Indian Ocean, which in turn help maintaining the warm pool by preventing the equatorial upwelling in the eastern Indian Ocean. The observed warm pool is thus better viewed as surface warm water piled from both sides of the maritime continent due to the wind stresses cooperatively over the western Pacific and the eastern Indian Ocean. The coupling between these two ocean basins has recently been extensively investigated for the interannual variability associated with ENSO (Klein et al. 1999; Lau and Nath 2000, 2003; Watanabe and Jin 2002, 2003). Several studies using coupled general circulation models (CGCM) further showed that the Indian Ocean is active in modulating the ENSO amplitude and periodicity (Yu et al. 2002; Wu and Kirtman 2004; Kug et al. 2006). These studies may advocate the necessity of dealing with the coupled atmosphere-ocean systems in the Pacific and Indian Oceans together in understanding the climatological mean state as well.

In this study, we attempt to demonstrate that the warm pool around the maritime continent is the product of the tropical atmosphere-ocean system in the Pacific and Indian Oceans *as a whole*, rather than the dynamical adjustment in the Pacific alone.

Furthermore, the extent to which the widely spread, single warm pool as observed is a unique solution in the coupled system is investigated by exploring the equilibrium or climatological states in a hierarchy of models, in which the tropical Pacific and Indian Oceans are as idealized as possible without loosing generality. In this Part I, a conceptual model for tropical oceans coupled with the Walker circulation is used to draw an outline of the hypothesis proposed throughout this study. A more comprehensive coupled model will be used in the companion paper (Watanabe 2007, referred to as Part II).

This paper is organized as follows. In the next section, a conceptual model for the tropical atmosphere-ocean system is described. The model has been proposed to explain the mean state and its variability primarily in the tropical Pacific, which is revised in this study. In section 3, equilibrium states of the simple tropical climate model are examined. Their stability and dependence on several control parameters are also presented. Section 5 gives a summary, discussion and remarks to Part II.

2. A simple tropical model

We use a simple tropical climate model proposed by J96. This model has two degrees of freedom for the ocean mixed layer temperature, or simply SST, in the eastern basin, T_e, and the departure of the thermocline depth from a reference depth in the western basin, h_w, respectively. The J96 model is regarded as a prototype to the so-called recharge oscillator model (Jin 1997) which is a well-known theoretical model for ENSO, but has an advantage that the solutions are obtained for the mean state but not for the anomaly from the mean state.

The eastern basin SST is controlled by

$$\frac{dT_e}{dt} = -\varepsilon_T (T_e - T_r) - \theta(w)\frac{T_e - T_{se}}{H_m} \quad , \tag{1}$$

where

$$\theta(w) = \begin{cases} w & \text{for } w > 0 \\ 0 & \text{otherwise} \end{cases} \quad .$$

The first term on the right hand side of (1) represents the net heating due to radiative and surface heat fluxes while the second term represents the dynamical cooling due to the equatorial upwelling. The net heating is simply expressed by the restoring of SST toward a zonally uniform, radiative-convective equilibrium temperature, T_r, with the timescale ε_T^{-1}. The dynamical cooling comes from the vertical advection at the base of the mixed layer, so that it depends on the subsurface temperature, T_{se}, prescribed mixed layer depth, H_m, and the upwelling velocity w. Note that the function $\theta(w)$ results from the upstream differencing, indicating that the upwelling cools the mixed layer but not vice versa.

The upwelling velocity is solely due to Ekman pumping, proportional to the zonal wind stress（τ）along the equator.

$$w = -\alpha_d \tau \quad , \tag{2}$$

where α_d can be determined by the oceanic momentum dissipation rate and β at the equator (Zebiak and Cane 1987). The zonal stress is decomposed into

$$\tau = \tau_0 - \mu(T_w - T_e) \quad , \tag{3}$$

where τ_0 is due to the Hadley circulation, therefore defined to be negative, while the second term is associated with the Walker circulation which is driven by the SST contrast between the eastern (T_e) and western (T_w) basins, the latter being assumed to

be in the radiative-convective equilibrium, namely, $T_w = T_r$. The relevance of this assumption will be discussed in section 4b. This part, when coupled with the thermocline change, is a key component of the climatological Bjerknes feedback. The parameter μ is the feedback coefficient which measures the efficiency of the zonal differential heating in driving the Walker circulation.

The subsurface temperature is strongly influenced by the thermocline depth in the eastern basin and may be parameterized as

$$T_{se} = T_r - (T_r - T_{r0}) \frac{1 - \tanh\left[(H + h_e - z_0) / h^* \right]}{2} \quad , \tag{4}$$

where T_{r0} is the temperature beneath the thermocline, z_0 the depth at which w takes its characteristic value, and h^* a measure of the thermocline sharpness. The thermocline depth in the eastern basin is given by $H + h_e$, where h_e is the departure from the reference depth, H , and determined by the integral of the Sverdrup relationship:

$$h_e = h_w + bL\tau \quad , \tag{5}$$

where $bL\tau$ is proportional to the zonally integrated wind stress and hence L is the ocean basin width and b is a parameter for the efficiency of wind stress in creating the thermocline tilt. The thermocline depth in the western basin, h_w, adjusts slowly to the zonally integrated Sverdrup mass transport that is proportional to the zonally integrated wind stress curl due to the basin-wide dynamical adjustment at a rate r,

$$\frac{dh_w}{dt} = -rh_w - \frac{rbL\tau}{2} \quad , \tag{6}$$

where the second term on the right hand side represents the zonally integrated Sverdrup mass transport, to which a factor $r/2$ has been multiplied so that equilibrium h_w and h_e

are $-bL\tau/2$ and $bL\tau/2$, respectively. The derivation and rationales of (6) have been given in more detail in J96.

Equations (1)-(6) form a closed set, in which the prognostic variables are only T_e and h_w. Following J96, constants are set to: $T_r = 303$ K, $T_{r0} = 291$ K, $\varepsilon_T = (75 \text{ days})^{-1}$, $r = (300 \text{ days})^{-1}$, $H_m = 50$ m, $H = 100$ m, $z_0 = 75$ m, $h^* = 50$ m, $\mu = 0.1$ N m^{-2} K^{-1}, and $\mu\alpha_d = 7.5$ m K^{-1} month^{-1}. The primary control parameters in this simple model are the coupled feedback coefficient, ocean basin width and the zonally uniform part of the wind stress that are all changeable for different ocean basin. In J96, they are combined as μbL and τ_0/μ, which are 12.5 m K^{-1} and -1 K for the tropical Pacific, 6.25 m K^{-1} and -1 K for the tropical Atlantic, and 6.25 m K^{-1} and +1 K for the tropical Indian Ocean, respectively. The stationary solutions can be calculated for each ocean and collectively plotted in Fig. 2a, which reproduces Fig. 1 of J96. In the equilibrium state the thermodynamic balance is achieved between the surface net heating and the dynamical cooling due to upwelling (right hand side of (1)), the latter being different from basin to basin (Fig. 2a).

The Bjerknes feedback is proportional to the zonal integral length of τ in (6) and to the coupled feedback in (3), so that more efficiently the upwelling cools SST as μbL becomes larger as in the Pacific. The equilibrium state of T_e is around 24 °C in the Pacific (intersection in Fig. 2a), which indicates a large zonal contrast in SST and the thermocline depth. When the basin length is reduced to half (or equivalently the coupled feedback weakened), which corresponds to the Atlantic Ocean, the cold tongue becomes warmer by about 3 degrees as in observations. Besides, the equatorial

upwelling is no longer effective in creating the cold tongue if the background wind stress, τ_0, is reversed, which mimics the tropical Indian Ocean.

On one hand, the J96 model captures the basic characters of the oceanic climatological mean states in a single set of equations. Furthermore, linearized equations for (1) and (6) exhibit that the Pacific mean state is unstable, leading to an ENSO-like oscillation while the other two oceans are not. Premising that the coupled feedback and the ocean dynamics commonly work to maintain the mean states and to generate anomalies from them, this model provides a dynamical basis to ENSO as well as the cold tongue. On the other hand, the model may have two concerns when arguing the dynamics of the warm pool. One is that the stationary states are independent of each other between the ocean basins; it is not consistent with the descriptive view of the warm pool as mentioned in the introduction. Another weakness is that τ_0 induced by the Hadley circulation must be negative at any situation, nevertheless, it has to be positive for the Indian Ocean; otherwise, cold tongue emerges there.

The Walker circulation is primarily forced by convective heating over the equatorial land region, which will accompany the convergence in the lower atmosphere (e.g., Stone and Chervin 1984). This convergence can couple two ocean basins via the atmospheric dynamics, leading to the surface easterly (westerly) to the east (west) of the active convections. We therefore extend the J96 model such as to include the coupling of two ocean basins as follows. First, two ocean basins, referred to as the first basin (placed to the west) and the second basin (placed to the east), are defined. Most of the equations (1)-(6) are the identical between the basins 1 and 2, except for the wind stress which is now expressed as

$$\tau_1 = \tau_0 - \mu(T_r - T_{e1}) + C \quad , \qquad (7)$$

$$\tau_2 = \tau_0 - \mu(T_r - T_{e2}) - C \quad , \tag{8}$$

where the subscripts '1' and '2' indicate variables in the basins 1 and 2, respectively, and C represents a convergence feedback which couples the two ocean basins as

$$C = \delta(\tau_1 - \tau_2) \quad . \tag{9}$$

We have implicitly assumed that the presence of land gives rise to this convergence feedback, which automatically generates positive τ_1 if the Bjerknes feedback in the basin 2 is strong enough. The convergence feedback is controlled by the parameter, δ, which is set to $\delta / \mu = 1.25$. This value determines the relative influence between the inter-basin temperature contrast and the temperature difference within the basin to the wind stress, which is changed in section 3c to explore the role of the inter-basin coupling in the model solutions. The basins 1 and 2 mimic the tropical Indian Ocean and the Pacific, so that we set $\mu b L_1$=6.17 and $\mu b L_2$=12.33 m K^{-1}, where L_i indicates the ith basin width, but with τ_0 / μ fixed at -1 K for both oceans. Two sets of Eqs. (1), (2), (4)-(6), in addition to (7)-(9), have four degrees of freedom and are referred to as the extended J96 model.

Figure 2b shows the equilibrium states as in Fig. 2a but for the extended J96 model with (solid) and without (dashed) the convergence feedback. In the absence of the convergence feedback, or the inter-basin coupling, equilibrium T_e in the Pacific, namely, T_{e2}, is identical to that in Fig. 2a while T_e in the Indian Ocean (basin 1) reveals a weak cold tongue same as in the Atlantic Ocean of the J96 model. The inter-basin coupling makes the Pacific cold tongue stronger and, by reversing the wind stress in the Indian Ocean, the Indian Ocean SST to the radiative-convective equilibrium temperature. The extended J96 model is thus shown to be relevant in obtaining the

warm pool between the Pacific and Indian Oceans as well as the strong cold tongue in the eastern Pacific with a reasonable definition to τ_0.

3. Two regimes in the simple tropical climate model

a. Stationary solutions

As argued in J96 and also shown in Fig. 2a, as the ocean basin length increases the dynamical cooling works more effectively in creating the cold tongue in the eastern basin. In the extended J96 model, convergence occurs over the land between the two basins when the cold tongue is only slightly weak (hence the zonal stress also weak through (7)) in the basin 1, resulting in a spontaneous emergence of the single warm pool between the two basins (Fig. 2b). It is therefore clear that the ratio between L_1 and L_2 is a critical parameter for the equilibrium states. In order to identify possible solutions of the extended J96 model, the parameter which represents the relative basin width is defined as

$$\alpha = \frac{L_2}{L_1} - 1 \quad . \tag{10}$$

The two ocean basins have equal length with $\alpha = 0$ while the "Pacific" is twice as large as the "Indian Ocean" with $\alpha = 1$, which is the case shown in Fig. 2b. In nature, α may be roughly estimated to be $1 \le \alpha \le 1.5$ although the precise value is hardly obtained because of the complicated land geometry. With the whole basin width, $L_t \equiv L_1 + L_2$, fixed at $\mu b L_t = 18.5$ m K^{-1}, stationary solutions can be presented as a function of α (Fig. 3). The model consists of a set of nonlinear equations, so that the stationary solution was first calculated at $\alpha = 0$ when the two oceans are identical, i.e., $C = 0$ in this particular solution, therefore the equilibrium T_e can be obtained as in Fig.

2. The stationary solution at slightly larger α is then computed from the initial guess given by the stationary state at $\alpha = 0$ using an iterative method. This procedure is repeated until $\alpha = 1.4$ to find a branch originating from the stationary state for the equal basin length. Another branch is also identified by first calculating the solutions at $\alpha = 1.4$ and then repeating with reduced α. Since we attempt to mimic the coupled Indo-Pacific climate, positive α cases are examined here. However, we can use negative α as well, possibly representing the coupled Pacific-Atlantic Oceans, which will be explored in section 3d.

The equilibrium T_e for the two basins is shown in Fig. 3, in which two branches of stationary states are identified. One is originating from the solutions with $\alpha = 0$ at which the mean states reveal a weak cold tongue identical between two oceans. As α increases the cold tongue is weakened but continues to be present in the basin 1. This implies that the warm pool is split into two at the western part of each ocean basin, so that we call this branch the *split warm pool regime*. This regime does not have stationary solutions beyond $\alpha \approx 0.7$, where another branch appears: the strong cold tongue in the Pacific accompanied by the radiative-convective equilibrium in the Indian Ocean, which are qualitatively the same as the state shown in Fig. 2b and therefore denoted as the *single warm pool regime*. In a range of $0.35 < \alpha < 0.7$, we also find multiple regimes, one of which is in reality selected depending upon the initial state.

Stability of the steady mean states shown in Fig. 3 is first examined by simply integrating the extended J96 model in time with an initial state slightly deviating from the equilibrium state. The trajectory for T_e in the two ocean basins is plotted against α in Fig. 4a, which indicates that the whole split regime and a part of the single warm pool regime are unstable, which give rise to the supercritical Hopf bifurcation around $\alpha = 0.9$.

The trajectory in such unstable regimes is far enough from the stationary state (denoted by triangles in Fig. 4a); with $\alpha = 0$ for instance, time series of T_e show that a vacillation between the strong cold tongue ($T_e < 22$ °C) and the radiative-convective equilibrium ($T_e = 30$ °C) is regularly taking place in the two oceans (Fig. 4b). In one particular ocean basin, the eastern basin SST and the western basin thermocline depth oscillate with an out-of-phase relationship, which has been found in the ENSO-like oscillatory solution of the recharge model (cf. Fig. 3b of Jin 1997) except for much larger amplitude in the extended J96 model (Fig. 4c). This oscillation occurs during the period that another ocean basin is in mostly radiative-convective equilibrium state (Fig. 4d). Once the eastern basin SST approaches the radiative-convective equilibrium temperature, it stays longer time and another ocean basin starts to warm up. This looks like a conventional coupled oscillation between two springs, but some nonlinearity must work since the warm states prolongs more than the cold states (Fig. 4b).

The reason why the split warm pool regimes are not stably equilibrated can be explained as follows. When the basin 2 swings toward the El Niño-like state, equatorial easterly is weakened and the resultant surface divergence anomaly over the land region, which may represent the suppressed convections there, necessarily accompanies intensified easterly in the basin 1 that eventually leads to the La Niña-like state. This coupled instability is prohibited as T_e in the basin 2 approaches the upper limit. As long as the Bjerknes feedbacks are similar in magnitude in the two basins, the La Niña-like state in one basin can significantly maintain the El Niño-like state in another basin. While the two basins are interchangeable in this simple model, the influence of one basin to another may not be symmetric in more complicated systems which explicitly represent the convectively coupled equatorial waves in the atmosphere. This asymmetry

will be highlighted in Part II.

b. Linear stability

A complete picture of the stability of the solutions in Fig. 3 can be obtained with a linearized version of the extended J96 model. Let **x** be the state vector

$$\mathbf{x}^T = \left(h'_{w1}, T'_{e1}, h'_{w2}, T'_{e2}\right) \quad , \tag{11}$$

which consists of perturbations (denoted by prime) for the prognostic variables in two ocean basins, the linearized equations are expressed in the matrix form.

$$\frac{d\mathbf{x}}{dt} + \mathbf{L}\mathbf{x} = 0 \quad , \tag{12}$$

where

$$\mathbf{L} = \begin{pmatrix} r & \frac{\varepsilon_A rbL_1}{2} & 0 & -\frac{\varepsilon_B rbL_1}{2} \\ -\gamma_1 & R_1 & 0 & \gamma_1 \varepsilon_B bL_1 + S_1 \\ 0 & -\frac{\varepsilon_B rbL_2}{2} & r & \frac{\varepsilon_A rbL_2}{2} \\ 0 & \gamma_2 \varepsilon_B bL_2 + S_2 & -\gamma_2 & R_2 \end{pmatrix} \tag{13}$$

Each term in (13) is, respectively,

$$\varepsilon_A = \mu \frac{1-\delta}{1-2\delta} \quad , \quad \varepsilon_B = \varepsilon_A \frac{\delta}{1-\delta} \tag{14}$$

$$R_i = \varepsilon_T + \frac{\theta(\overline{w}_i)}{H_m} - \varepsilon_A bL_i \gamma_i - \frac{\mathcal{H}(\overline{w}_i)\alpha_d \mu}{1-\delta} \frac{\overline{T}_{e_i} - \overline{T}_{se_i}}{H_m} \quad , \quad i = 1, 2 \tag{15}$$

$$S_i = \frac{\mathcal{H}(\overline{w}_i)\alpha_d \mu \delta}{(1-\delta)^2} \frac{\overline{T}_{e_i} - \overline{T}_{se_i}}{H_m} \quad , \quad i = 1, 2 \tag{16}$$

$$\gamma_i = \frac{\theta(\overline{w}_i)}{H_m} \left. \frac{d\overline{T}_{se}}{dh_e} \right|_{h_e = h_{ei}} \quad , \quad i = 1, 2 \tag{17}$$

where the overbar denotes the stationary state, *i* the index of ocean basins, and $\mathcal{H}(x)$ is the Heavyside function of *x*. It should be noted that in the absence of the inter-basin coupling, i.e., $\delta = 0$, **L** is reduced to a block diagonal matrix, indicating that two ocean basins are independent of each other.

Eigenmodes of **L** are numerically obtained separately for each α. The growth rate and frequency for the most unstable modes are then plotted in a similar manner to the stationary solutions (Fig. 5). Consistent with Fig. 4a, all the steady states in the split regime and a part of the single regime are found to be linearly unstable. The split regime is generally more unstable than the single regime since the convergence feedback can destabilize the system as qualitatively described in the previous subsection. In the single warm pool regime, the convergence is driven solely by the wind stress in the basin 2 (Pacific) because of $T_{e1} = T_r$. It is not quite clear why the most unstable mode emerges with $\alpha = 0.4$, but the reason may be speculated as follows. The positive feedback induced by the inter-basin coupling is the strongest with $\alpha = 0$ while the conventional Bjerknes feedback works more efficiently with larger α. The steady mean state may therefore be the most unstable with an intermediate value of α. In the most part of the single warm pool regime, the leading eigenmode is, regardless of its growth rate, oscillatory with the period between 1.9 and 2.9 years. The oscillation at the neutral mean state with $\alpha = 0.9$ has the periodicity of 2 years, which is somewhat shorter than that in J96 but still appears to represent the prototype of ENSO. As in the J96 model, the Bjerknes feedback is reduced for a too strong cold tongue, so that the steady states with extremely large α are stable and do not reveal any oscillatory eigenmode.

c. Sensitivity to the convergence feedback

As demonstrated previously, the convergence feedback acts to maintain the stable single warm pool for $\alpha \geq 0.9$ with the prescribed coefficient of the inter-basin coupling, $\delta / \mu = 1.25$. This coefficient is, however, tunable and the equilibrium state is switched to the split regime with $\delta = 0$ (Fig. 2b). We therefore explored how the mean state depends on this convergence feedback, which now varies from 0 to 2. The equilibrium T_e with $\alpha = 1$ is plotted as a function of δ / μ in Fig. 6, which again reveals two distinct regimes: an unstable split regime with $\delta / \mu < 1.2$ and a stable single warm pool regime with larger δ / μ. Compared to the regime dependence on α (Fig. 3), the regime transition in Fig. 6 is smoother and no hysteresis occurs, indicating that the convergence feedback is a crucial piece in stabilizing the single warm pool regime in the simple model while the stationary solutions are more sensitive to the relative basin width than to the magnitude of the inter-basin coupling.

d. Coupling with the "Atlantic" Ocean

Insofar, we have used the extended J96 model with positive α, namely, the basin 2 equal to or grater than the basin 1, which mimics the coupled Pacific and Indian Oceans. The same model but with negative α may represent the coupled Pacific and Atlantic Oceans, in which the basin 1 (basin 2) will be assigned to the tropical Pacific (Atlantic). Assuming that the Pacific is twice as large as the Atlantic, the observational estimate will be $\alpha \approx -0.5$ (cf. Eq. (10)).

The regime diagram with negative α is roughly a mirror to Fig. 3 (not shown); the single (split) warm pool regime occurs with smaller (larger) α. The observed Atlantic climatology reveals a weak cold tongue and a small warm pool (Fig. 1), so that the split regime which exists around $\alpha = -0.4$ may be of relevance. However, the split

regime in the coupled Pacific-Atlantic vacillates as in the counterpart in the coupled Pacific-Indian Ocean, which is an unrealistic feature never observed, suggesting that the extended J96 model does not capture the observed mean state in the tropical Atlantic due to lack of other important processes.

In nature, Pacific, Indian and Atlantic Oceans are all coupled and likely to interact with each other. Since the Pacific warm pool is much larger than the Atlantic one, coupling of three ocean basins may better represent the mean state in the equatorial Atlantic. We therefore coupled the third basin (basin 3) which mimics the Atlantic Ocean to the extended J96 model and then re-examined the equilibrium states. The governing equations for the basin 3 are the same as the other basins, in which the inter-basin coupling term consists of the zonal stress difference with the other two basins. For simplicity, width of the basin 3 is prescribed to $L_t/2$ and the relative width between the basins 1 and 2 (the Indian Ocean and the Pacific) is changed with α as in section 3a. This experimental setup will be used in a GCM study of Part II. Note that the three basins have the identical width at $\alpha = 0$.

The stationary solutions of this coupled three-ocean system are calculated with the standard magnitude of the inter-basin coupling of $\delta/\mu = 1.25$ (Fig. 7a). At $\alpha = 0$, three sets of equilibria are identified: cold tongue generated in all the basins (T_e=26.6 °C), one basin in the radiative-convective equilibrium while the other two basins having the cold tongue (T_e=25.1 °C), and two basins in the radiative-convective equilibrium while one basin having the cold tongue (T_e=23.0 °C). The first equilibrium solutions may be the "pure" split regime, where all the ocean basins actually vacillate with the temporal phase leading/lagging by $\pi/3$ to each other; however, this state disappears at

$\alpha > 0$. The second solutions also correspond to the unstable split regime in which the vacillation occurs between two basins and the rest ocean weakly oscillates around the radiative-convective equilibrium. In these regimes the Pacific cold tongue becomes stronger as α increases, but they switch to the third solutions corresponding to the single warm pool regime at around $\alpha = 0.2$ (Fig. 7a).

Compared to the two-ocean system (Fig. 3), the three-ocean system has more equilibria, among which the single regime is the dominant state. It is also found by comparing Figs. 3 and 7 that the interactive Atlantic works to stabilize the system such as to keep the strong Pacific cold tongue. In this regime, however, the Atlantic Ocean is yet in the radiative-convective equilibrium. When the inter-basin coupling that also acts to stabilize the system (Fig. 6) is slightly weakened to $\delta / \mu = 1$, the stable regime is confined to $\alpha \geq 0.45$, in which the Atlantic T_e decreases from T_r by 2-3 degrees, indicating the presence of the weak cold tongue (Fig. 7b; note that the second solutions are not plotted to avoid the diagram being too busy).

Assuming that the wind convergence induced by the SST contrast is less effective over a wide continent such as Africa and South America, we then reduced δ / μ to half between the Indo-Atlantic and the Pacific-Atlantic basins. The regime diagram obtained with the above condition is displayed in Fig. 7c. Two regimes in the Indo-Pacific Ocean are quite similar to those found in Fig. 3 and accompany the weak cold tongue in the Atlantic. One difference from the two-ocean system is that both the regimes are linearly unstable for $0 \leq \alpha \leq 1.4$, which may rather be reasonable because the stable single regime cannot generate ENSO autonomously (cf. J96). In fact, time evolution of T_e in the three oceans at $\alpha = 1.2$ in the model shown in Fig. 7c reveals the interannual variability prevailing with about 3-5yr period in both the Pacific and the

Atlantic (Fig. 8). They are reminiscent of the observed ENSO and the "Atlantic Niño" (e.g., Zebiak 1993) besides the Pacific warm state intermittently bursts to almost 30 °C, when the Indian Ocean shows a weak cold state. This will be an indication of the ghost of unstable split regime, which may provide an alternative mechanism of the El Niño bursting (Timmermann et al. 2003).

4. Summary and discussion

a. Summary of Part I

Motivated by the fact that the Pacific warm pool spreads to the eastern Indian Ocean and also by recent studies which show the active role of the Indian Ocean SST variability in the Pacific ENSO cycle, this study aims at understanding the possible role of the interaction between the two oceans in establishing the climatological mean warm pool. In this Part I, we extend the Jin's (1996) simple coupled model for one ocean basin such as to incorporate the coupling of two oceans via the Walker circulation and then explored the equilibrium states and their stability with varying parameters of the inter-basin coupling and the relative ocean width.

When the inter-basin coupling is sufficiently strong, surface convergence over the maritime continent associated with the easterly winds over the Pacific acts to generate the equatorial westerly over the Indian Ocean, which gives rise to a spontaneous emergence of the warm pool between the two ocean basins. Furthermore, the simple system suggests that tropical climate has two equilibria depending upon the ocean basin widths. One is the single warm pool regime corresponding to current climate and another is the split warm pool regime which accompanies warm pools created at the western sides of each ocean basin. While the split regime can occur

when two oceans are relatively close in basin width, such a regime is found to be unstable due to the inter-basin coupling and hence exhibit a large-amplitude vacillation between ocean basins, each of which is amplified by the Bjerknes feedback. The above two regimes of the equatorial warm pool are also identified in the coupled three-ocean system which includes the Atlantic Ocean.

b. Discussion and remarks to Part II

The presence of the multiple equilibria of the tropical atmosphere-ocean system has been reported in previous studies (e.g., J96, Sun and Liu 1996, Timmermann et al. 2003) in the absence of the inter-basin coupling. In the J96 model, for example, if the coupled feedback parameter, μbL, is eventually reduced from the Atlantic value (6.25 m K^{-1}) then we obtain two equilibria of the weak cold tongue state and the radiative-convective equilibrium in the entire ocean, the latter being linearly unstable (cf. Fig. 2a). The two regimes of the warm pool obtained from the extended J96 model are conceptually different from such results dealing with one ocean basin since the convergence feedback is crucial in producing the single warm pool regime. When we change μ in our extended J96 model as has been done in simple model studies for ENSO, stable branch of the radiative-convective equilibrium state is obtained. Such solutions are, however, trivial and independent of the inter-basin coupling.

One of the controversial simplifications of the model may be the western basin SST which is assumed to be always in the radiative-convective equilibrium (cf. section 2). Because of this, the Indian Ocean SST in the single warm pool regime is uniform throughout the basin in the simple model, which may be too crude to represent the observed Indian Ocean climatology. In reality, the super-rotating surface wind induces

the upwelling in the western tropical Indian Ocean, at slightly south of the equator, which results in a coherence between the subsurface temperature and SST (Xie et al. 2002). Simple model also shows that the cold tongue in the western basin is possible to appear with a certain value of the coupling coefficient (Dijkstra and Neelin 1995). We therefore examined the equilibrium solutions in the model in which the western basin SST, T_w, is allowed to vary due to the upwelling as in (1). The results did not alter the conclusions obtained here, namely, the steady mean states were quite similar to those shown in Fig. 3, except for the equilibrium T_w in the Indian Ocean cooler by 1-2 K than T_r only in the single warm pool regime. As will be shown in Part II, results in more complicated coupled model are indeed consistent with the solutions of the extended J96 model, which further justifies that the assumption can be crudely accepted.

The inter-basin coupling appears to have two different roles in the regime behavior of the conceptual model. The coupled vacillation between the two basins found in the split regime is crucially dependent upon the inter-basin coupling, which actually favors the single warm pool regime (Fig. 2b). In fact, stronger the convergence feedback is, the stable single regime occupies in a wider range of α (Figs. 6 and 7ab). The stable regime, however, may not be realistic since it cannot generate an ENSO-like interannual variability without external forcing. While the question whether ENSO is a self-sustained oscillation or stochastically excited variability may still be controversial, the unstable single regime with moderate strength of the inter-basin coupling seems to match observations in terms of the mean state and the interannual variability (Figs. 7c and 8). As presented in section 3d, the interactive Atlantic Ocean brings a richer behavior of the equilibrium solutions than in the coupled Indo-Pacific system shown in section 3a-c. While the overall regimes are similarly identified both in the two-ocean

and the three-ocean systems, coupling with the interactive Atlantic does affect the regime transition and stability, as will be shown with a CGCM in Part II.

Presence of regimes in simple tropical climate models such as one used in this Part I crucially depends on how to represent the nonlinear ocean dynamic feedback associated with the thermocline tilt and the upwelling. There is some arbitrariness on this regard, so that the results presented here must be validated using a model having much larger degrees of freedom, which is the work we have done in Part II.

Acknowledgments. The author is grateful to Drs. F.-F. Jin and A. Timmerman for stimulating discussion and their constructive comments. Thanks are also due to Drs. J. P. McCreary, S.-P. Xie, N. Schneider, B. Qiu, J.-S. Kug and anonymous reviewers who provided valuable comments. This work was partly supported by a Grant-in-Aid for Scientific Research from MEXT, Japan.

REFERENCES

Bjerknes, J., 1969: Atmospheric teleconnections from the equatorial Pacific. *Mon. Wea. Rev.*, **97**, 163-172.

Clement, A. C., R. Seager, M. A. Cane, and S. E. Zebiak, 1996: An ocean dynamical thermostat. *J. Climate*, **9**, 2190-2196.

Clement, A. C., R. Seager, and R. Murtugudde, 2005: Why are there tropical warm pools? *J. Climate*, **18**, 5294-5311.

Dijkstra, H. A, and J. D. Neelin, 1995: Ocean-atmosphere interaction and the tropical climatology. Part II: Why the Pacific cold tongue is in the east. *J. Climate*, **8**, 1343-1359.

Hartmann, D. L., and M. L. Michelsen, 1993: Large-scale effects on the regulation of tropical sea surface temperature. *J. Climate*, **6**, 2049-2062.

Held, I. M., 2001: The partitioning of the poleward energy transport between the tropical ocean and atmosphere. *J. Atmos. Sci.*, **58**, 943-948.

Jin, F.-F., 1996: Tropical ocean-atmosphere interaction, the Pacific cold tongue, and the El Niño-Southern Oscillation. *Science*, **274**, 76-78.

Jin, F.-F., 1997: An equatorial ocean recharge paradigm for ENSO. Part I: Conceptual model. *J. Atmos. Sci.*, **54**, 811-829.

Klein. S. A., B. J. Soden, and N.-C. Lau, 1999: Remote sea surface temperature variations during ENSO: Evidence for a tropical atmospheric bridge. *J. Climate*, **12**, 917-931.

Kug, J.-S., T. Li, S.-I. An, I.-S. Kang, J.-J. Luo, S. Masson, and T. Yamagata, 2006: Role of the ENSO-Indian Ocean coupling on ENSO variability in a coupled GCM *Geophys. Res. Lett.*, **33**, doi:10.1029/2005GL024916.

Lau, N.-C., and M. J. Nath, 2000: Impact of ENSO on the variability of the Asian-Australian monsoons as simulated in GCM experiments. *J. Climate*, **13**, 4287-4309.

Lau, N.-C., and M. J. Nath, 2003: Atmosphere-ocean variations in the Indo-Pacific sector during ENSO episodes. *J. Climate*, **16**, 3-20.

Li, T., T. F. Hogan, and C.-P. Chang, 2000: Dynamic and thermodynamic regulation of ocean warming. *J. Atmos. Sci.*, **57**, 3353-3365.

Neelin, J. D., and H. A. Dijkstra, 1995: Ocean-atmosphere interaction and the tropical climatology. Part I: The dangers of flux-correction. *J. Climate*, **8**, 1325-1342.

Neelin, J. D., and Co-authors, 1998: ENSO theory. *J. Geophys. Res.*, **103**, 14261-14290.

Pierrehumbert, R. T., 1995: Thermostats, radiator fins, and the runaway greenhouse. *J. Atmos. Sci.*, **52**, 1784-1806.

Ramanathan, V., and W. Collins, 1991: Thermodynamic regulation of ocean warming by cirrus clouds deduced from observations of the 1987 El Niño. *Nature*, **351**, 27-32.

Ramanathan, V., and Co-authors, 1995: Warm pool heat budget and shortwave cloud forcing: A missing physics? *Science*, **267**, 499-503.

Schneider, N., T. Barnett, M. Latif, and T. Stockdale, 1996: Warm pool physics in a coupled GCM. *J. Climate*, **9**, 219-239.

Seager, R., and R. Murtugudde, 1997: Ocean dynamics, thermocline adjustment, and regulation of tropical SST. *J. Climate*, **10**, 521-534.

Stone, P. H., and R. M. Chervin, 1984: The influence of ocean surface temperature gradient and continentality on the Walker circulation. Part II: Prescribed global changes. *Mon. Wea. Rev.*, **112**, 1524-1534.

Sun, D.-Z., and Z. Liu, 1996: Dynamic ocean-atmosphere coupling: A thermostat for the tropics. *Science*, **272**, 1148-1150.

Timmermann, A., F.-F. Jin, and J. Abshagen, 2003: A nonlinear theory for El Niño bursting. *J. Atmos. Sci.*, **60**, 152-165.

Wallace, J. M., 1992: Effect of deep convection on the regulation of tropical sea surface

temperature. *Nature*, **357**, 230-231.

Watanabe, M., and F.-F. Jin, 2002: Role of Indian Ocean warming in the development of the Philippine Sea anticyclone during ENSO. *Geophys. Res. Lett.*, **29**, 1478, doi:10.1029/2001GL014318.

Watanabe, M., and F.-F. Jin, 2003: A moist linear baroclinic model: Coupled dynamical-convective response to El Niño. *J. Climate*, **16**, 1121-1139.

Watanabe, M., 2007: Two regimes of the equatorial warm pool. Part II: Hybrid coupled GCM experiments. *J. Climate*, submitted.

Wu, R., and B. P. Kirtman, 2004: Understanding the impacts of the Indian Ocean on ENSO variability in a coupled GCM. *J. Climate*, **17**, 4019-4031.

Xie, S.-P., H. Annamalai, F. A. Schott, and J. P. McCreary, 2002 : Structure and mechanisms of South Indian Ocean climate variability. *J. Climate*, **15**, 864-878.

Yu, J.-Y., C. R. Mechoso, C. McWilliams, and A. Arakawa, 2002: Impacts of the Indian Ocean on the ENSO cycle. *Geophys. Res. Lett.*, **29**, 1204, doi:10.1029/2001GL014098.

Zebiak, S. E., and M. A. Cane, 1987: A model El Niño-Southern Oscillation. *Mon. Wea. Rev.*, **115**, 2262-2278.

Zebiak S. E., 1993: Air–sea interaction in the equatorial Atlantic region. *J. Climate*, **6**, 1567–1586.

FIGURE CAPTIONS

Fig.1 Annual mean climatology of SST (top), subsurface temperature (middle) and the zonal stress (bottom) along the equator. The contours of 26 °C (28 °C) are indicated in the top panel.

Fig.2 (a) Stationary solutions to the simple coupled model. Rates of the net heating (thin straight line with reversed sign) and dynamical cooling (thick curves) are plotted against T_e under the dynamical equilibrium. The stationary state is indicated by the intersection points. Note that the three curves mimicking the Pacific, Atlantic and Indian Oceans, respectively, are separately calculated. (b) As in (a) but for the solutions with the inter-basin coupling between the Pacific and the Indian Oceans (solid) compared to the solution without coupling (dotted).

Fig.3 Stationary solutions for T_e in the Pacific (circles) and Indian (squares) Oceans as a function of α with prescribed coefficients of the inter-basin coupling. Search of the two branches are started from the solutions at $\alpha = 0$ and $\alpha = 1.4$, respectively (indicated by arrows).

Fig.4 (a) Trajectory plots for T_e (dots) imposed on the stationary solutions (bold triangles) as a function of α. The black (grey) marks indicate the split warm pool (single warm pool) regime. (b) Time series of T_e in the Pacific (solid) and the Indian Ocean (dashed) with α=0. (c) Trajectory plots for T_e and h_w in the Indian Ocean. (d) As in (c) but for T_e in the two ocean basins.

Fig.5 Linear stability of the simple coupled model as a function of α. The open (closed) marks indicate growth rate (frequency) for the most unstable eigenmode,

obtained when the model is linearized with respect to stationary states in the split (triangle and square) and single (circle) warm pool regimes, respectively.

Fig.6 As in Fig. 3 but for varying inter-basin coupling coefficient δ / μ, with α prescribed to 1.0. The open (closed) marks indicate the stationary solutions linearly unstable (stable).

Fig.7 Regime diagram in the coupled three-ocean system with different convergence feedback parameters: (a) $\delta / \mu = 1.25$, (b) $\delta / \mu = 1$ and (c) $\delta / \mu = 1$ for the Indo-Pacific and $\delta / \mu = 0.5$ for the other basin coupling. Stationary solutions for T_e in the Pacific (circles), Atlantic (triangles) and Indian (squares) Oceans are plotted as a function of α. Stable (unstable) solutions are indicated with sold (open) marks.

Fig.8 Time evolution of T_e in the Pacific (thick solid), Atlantic (thin solid) and Indian Ocean (dashed) at $\alpha = 1.2$ in the experiment shown in Fig. 7c.

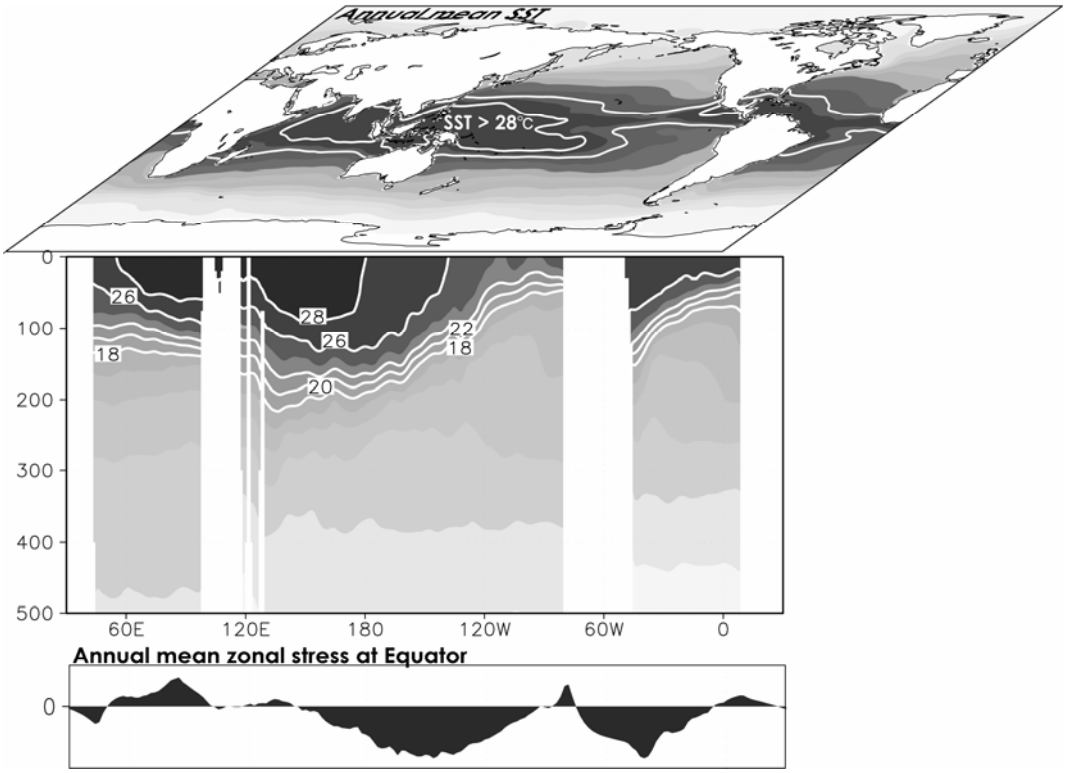

Fig.1 Annual mean climatology of SST (top), subsurface temperature (middle) and the zonal stress (bottom) along the equator. The contours of 26 °C (28 °C) are indicated in the top panel.

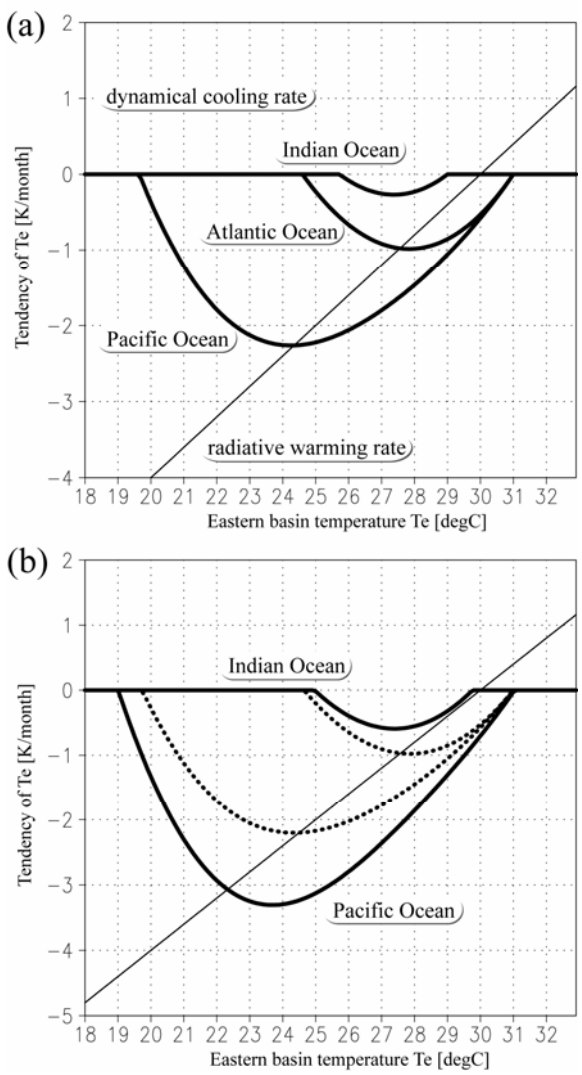

Fig.2 (a) Stationary solutions to the simple coupled model. Rates of the net heating (thin straight line with reversed sign) and dynamical cooling (thick curves) are plotted against T_e under the dynamical equilibrium. The stationary state is indicated by the intersection points. Note that the three curves mimicking the Pacific, Atlantic and Indian Oceans, respectively, are separately calculated. (b) As in (a) but for the solutions with the inter-basin coupling between the Pacific and the Indian Oceans (solid) compared to the solution without coupling (dotted).

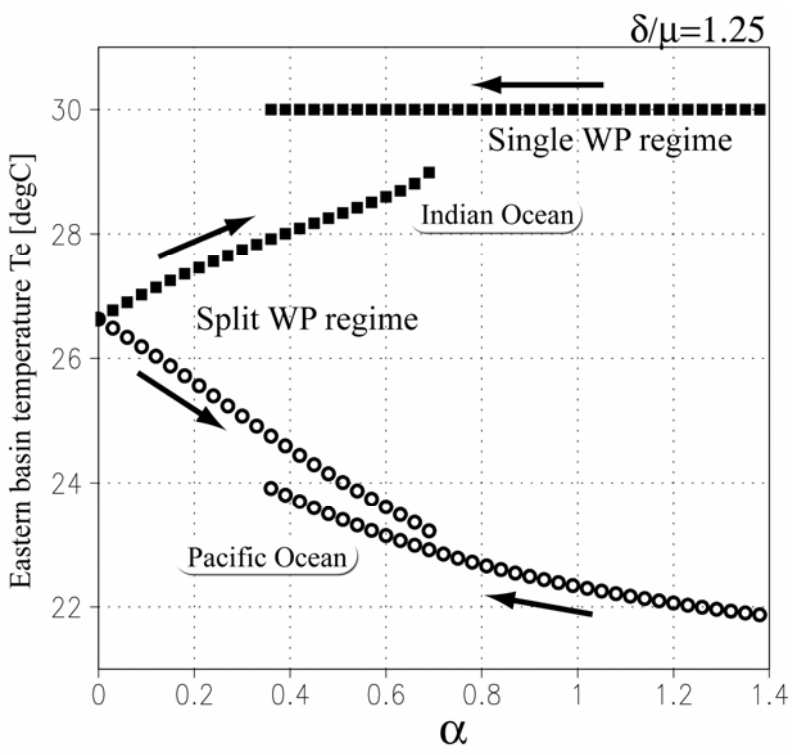

Fig.3 Stationary solutions for T_e in the Pacific (circles) and Indian (squares) Oceans as a function of α with prescribed coefficients of the inter-basin coupling. Search of the two branches are started from the solutions at $\alpha = 0$ and $\alpha = 1.4$, respectively (indicated by arrows).

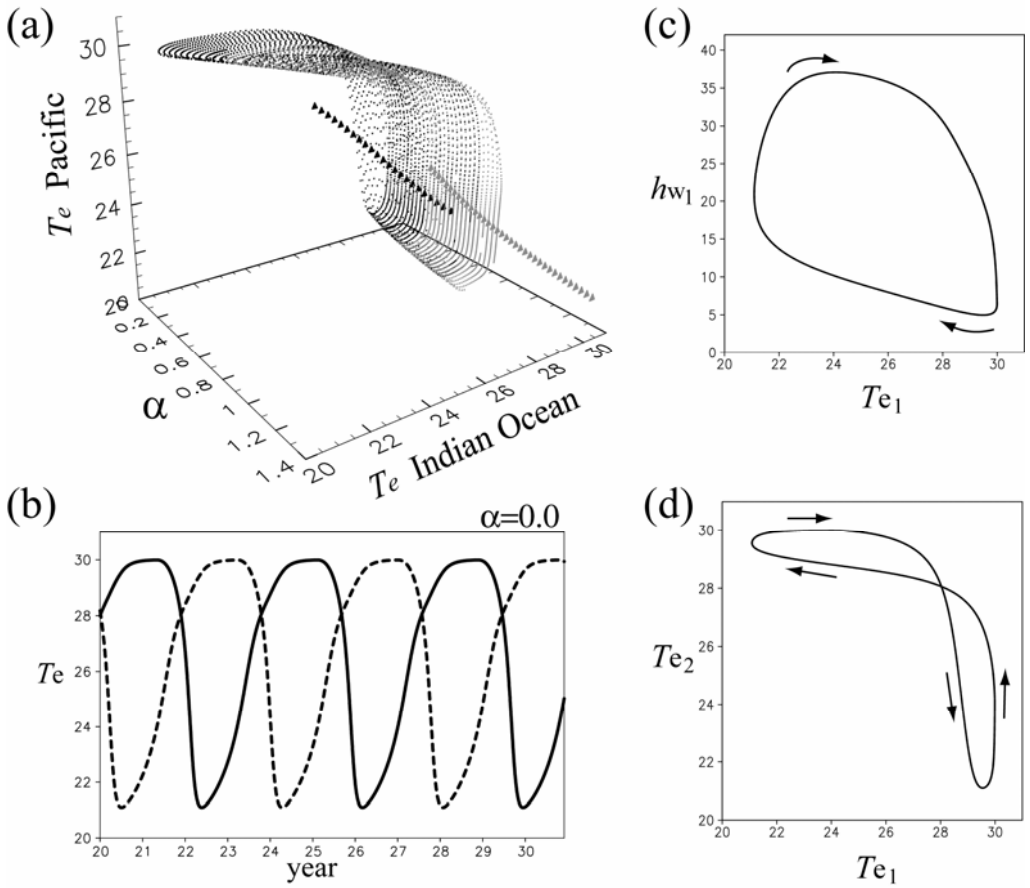

Fig.4 (a) Trajectory plots for T_e (dots) imposed on the stationary solutions (bold triangles) as a function of α. The black (grey) marks indicate the split warm pool (single warm pool) regime. (b) Time series of T_e in the Pacific (solid) and the Indian Ocean (dashed) with α=0. (c) Trajectory plots for T_e and h_w in the Indian Ocean. (d) As in (c) but for T_e in the two ocean basins.

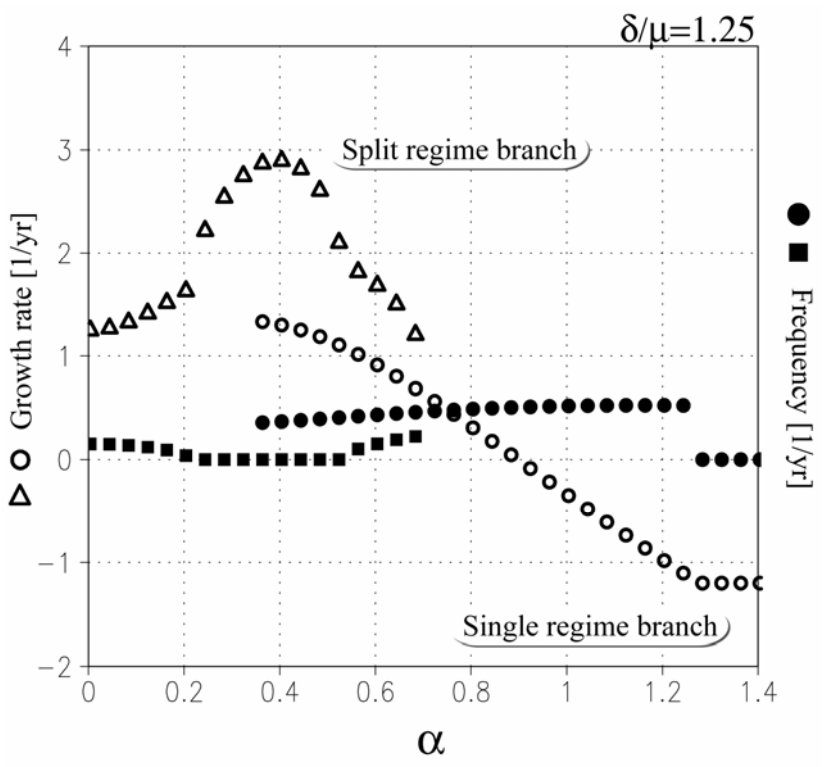

Fig.5 Linear stability of the simple coupled model as a function of α. The open (closed) marks indicate growth rate (frequency) for the most unstable eigenmode, obtained when the model is linearized with respect to stationary states in the split (triangle and square) and single (circle) warm pool regimes, respectively.

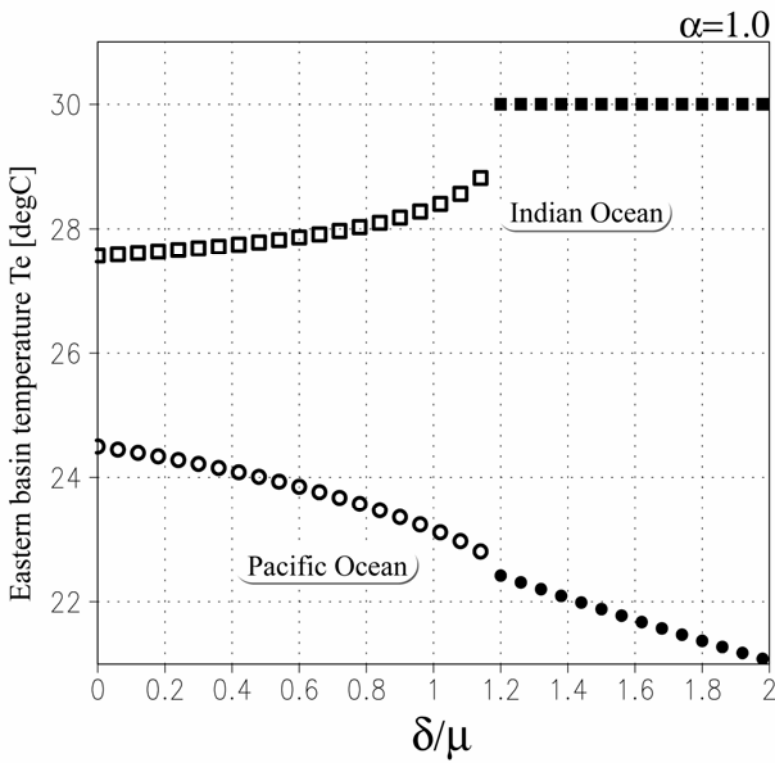

Fig.6 As in Fig. 3 but for varying inter-basin coupling coefficient δ / μ, with α prescribed to 1.0. The open (closed) marks indicate the stationary solutions linearly unstable (stable).

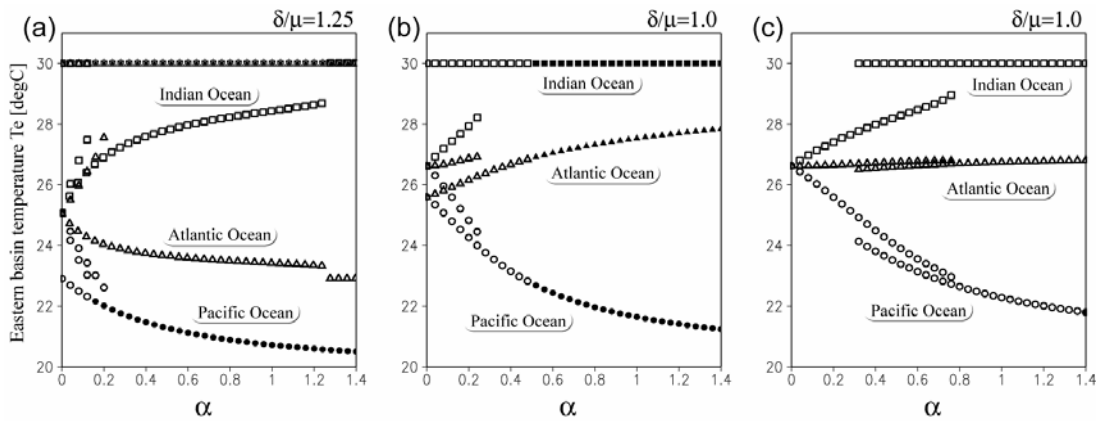

Fig.7 Regime diagram in the coupled three-ocean system with different convergence feedback parameters: (a) $\delta/\mu = 1.25$, (b) $\delta/\mu = 1$ and (c) $\delta/\mu = 1$ for the Indo-Pacific and $\delta/\mu = 0.5$ for the other basin coupling. Stationary solutions for T_e in the Pacific (circles), Atlantic (triangles) and Indian (squares) Oceans are plotted as a function of α. Stable (unstable) solutions are indicated with sold (open) marks.

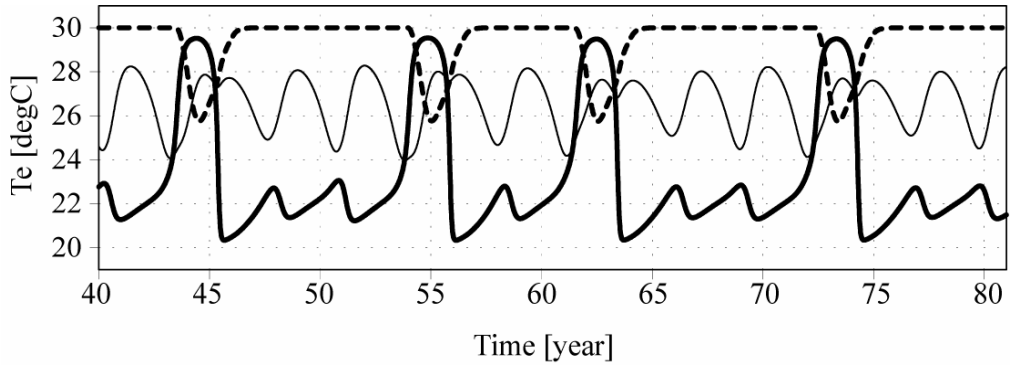

Fig.8 Time evolution of T_e in the Pacific (thick solid), Atlantic (thin solid) and Indian Ocean (dashed) at $\alpha = 1.2$ in the experiment shown in Fig. 7c.